




Research Article

Long-Term Characterization of Indoor Air Quality at a Research Area Building: Comparing Reference Instruments and Low-Cost Sensors

Mariarosaria Calvello ¹, Francesca Agresti,^{1,2} Francesco Esposito ², and Giulia Pavese ¹

¹*Institute of Methodologies for Environmental Analysis, Italian National Research Council, C. da S. Loja 85050, Tito Scalo, Potenza, Italy*

²*Basilicata University, Engineering School, C. da Macchia Romana, 85100 Potenza, Italy*

Correspondence should be addressed to Mariarosaria Calvello; mariarosaria.calvello@imaa.cnr.it

Received 20 March 2023; Revised 3 October 2023; Accepted 16 January 2024; Published 23 February 2024

Academic Editor: Xiaohu Yang

Copyright © 2024 Mariarosaria Calvello et al. This is an open access article distributed under the Creative Commons Attribution License, which permits unrestricted use, distribution, and reproduction in any medium, provided the original work is properly cited.

Indoor particle number size distribution (0.3–10 μm), equivalent black carbon (eBC), and Ångström absorption exponent (AAE) data were collected in real conditions, over a ten-month period at a research area building, in a semirural site, to characterize indoor aerosol loading. Additionally, during the campaign, emissions from four indoor sources commonly used at the site (incense, traditional cigarettes, electronic cigarettes, and heat-not-burn products) were studied during short-term experiments with the support of ultrafine particle (UFP) monitoring. Two particle low-cost sensors (PM LCS), Sensirion SPS30 (0.3–10 μm), were evaluated in the long-term campaign and during fast emission processes, to assess their accuracy and reliability. Penetration and infiltration of both fine and coarse particles from outdoor traffic, domestic heating, and dust resuspension were inferred as the main sources of indoor aerosols on a long-term basis. Moreover, long-range transported dust aerosols were found to influence indoor coarse number concentration. Among the source events, heat-not-burn (HNB) product resulted in the lowest effect on indoor air quality, whereas the highest AAE values from incense and traditional cigarettes suggest the brown carbon (BrC) production. The highest emission of UFP was caused by electronic cigarettes (e-cig), which spanned particles from the ultrafine to the coarse fractions. This was likely due to the release of metal and silicate from the coil. Analysis of number size distributions of the four experiments revealed the emission of fine particles (0.3–1 μm) and super micron particles. SPS30s performance was satisfactory in terms of accuracy, precision, and durability, indicating that these devices are suitable for monitoring indoor air quality. Additionally, the two PM LCS were able to detect all simulated fast emission sources.

1. Introduction

Indoor air pollution has a more detrimental effect on human well-being than outdoor pollution since people spend a major portion of their time in indoor environments. In their review, [1] estimated 1.8 million deaths associated with household air pollution in 2017. Despite this, in contrast to ambient air quality, there is no standard regulation worldwide for indoor air quality except for a few countries and regions (e.g., Canada, China, Portugal, and Taiwan) as reported in [2]. In their work, authors list the existing

national indoor air quality (IAQ) standards and discuss the World Health Organization (WHO) guidelines related to IAQ [3].

According to [4], people spend on average most of their time at home (58–69%), followed by work environments (28%). Among working places, offices constitute the most widespread professional environment, especially in industrialized countries, where about 67% of the workers are office employees [5]. The main sources of indoor particles in homes and offices are outdoor particle penetration, smoking, including new generation devices (e-cigs or HNB products),

cooking, and burning incense and candles [4, 6]. In recent years, several studies have established how each of these sources poses a risk for human health based on measurements of hazardous compounds such as polycyclic aromatic hydrocarbons (PAHs), volatile organic compounds (VOCs), formaldehyde, UFP, and black carbon (BC) [7–10].

In many cases, the metric used for the evaluation of indoor pollution impact is the mass of particles, often derived by converting number of particles to mass data from real-time optical counters. However, the choice of a density factor for the conversion is arbitrary when no simultaneous measurements with a reference instrument are available [11, 12]. Moreover, most indoor sources significantly increase particle number concentration (NC) with negligible impact on mass, especially when UFP are involved, and the knowledge of NC is necessary to predict the penetration and deposition dose in the human respiratory tract [13–15].

Generally, studies on indoor sources are conducted in test chambers and, only in a minor part, in real-life conditions [16–20] owing to the limitations associated with uncontrolled and unrepeatable experimental conditions. On the other hand, measurements carried out in real environments permit to evaluate the potential impact of aerosol transformation processes on indoor air quality [21, 22]. An example could be the possibility to better characterize second and third hand smoking exposure as described in [17].

Studies on indoor air quality are usually based on short-term datasets, thus not receiving epidemiologists' requests of long-term studies [23–25]. Conducting exposure studies to quantify indoor air quality would also require high spatial resolution, which is often unfeasible indoors due to the high cost, dimensions, noise, nuisance, and low portability of traditional instrumentation. In recent years, the use of PM LCS for indoor air quality monitoring has grown rapidly, helping to address these issues, and increasing the feasibility of a more widespread monitoring [26–29].

LCS implies, however, the collection of data with limited accuracy compared to reference instruments [30, 31, 32, 33, 34]. Although many efforts have been made to assess the state of the art about LCS, there is currently a lack of uniformity in the methods to evaluate their performance and to calibrate them [35–37]. The US EPA has developed a report to provide a reliable methodology for sensor performance evaluation, including testing protocols, metrics, and target values [38–40]. For Europe, the technical specification “CEN/TC 264/WG 42 – Air quality sensors” is developing a technical guide for data quality objectives to be achieved by PM LCS and is expected to be released in the near future [41–43]. Both documents focus mainly on outdoor applications. As regards indoor use of PM LCS, some reviews were produced within the scientific community describing various measurement campaigns carried out using PM LCS or trying to assess their performance [44–47]. Giordano et al. [45] suggested performing multiple tests to assess sensor linearity in their response to different aerosol sources. Ródenas García et al. [47] highlighted the potentiality and opportunity of LCS used indoor, indicating as a forthcoming requirement, the development of LCS for UFP and nanoparticles.

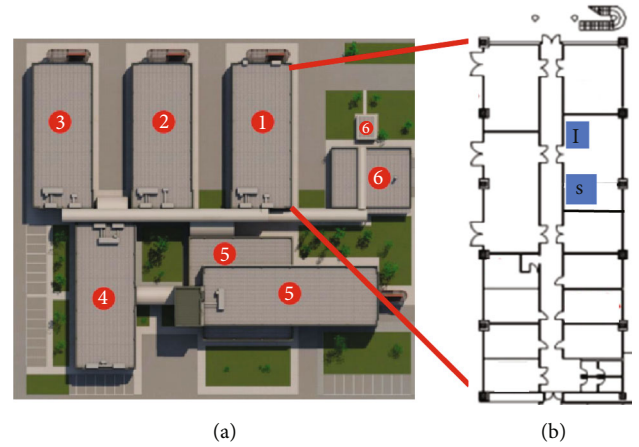


FIGURE 1: (a) General plan of the complex building hosting the Potenza research area. (b) Plan view of edifice 1 with the laboratory/office where the measurements were carried out. The red letters “I” and “S” indicate where the instruments and the sources were placed, respectively.

The aim of the present work is the long-term characterization of indoor aerosols in a laboratory, inside a research building. Short-duration high-emission events caused by four commonly used indoor sources (incense, traditional cigarette, e-cigs, and HNB) are also included in the analysis. In view of the possible future set-up of a low-cost network for indoor air quality control, two low-cost sensors were used together with the scientific instruments and their performances were evaluated along the measurement period. The aerosol characterization was carried out measuring particle number size distributions in the range $0.3\text{--}1\text{ }\mu\text{m}$ and eBC for a ten-month period, using a TSI Optical Particle Sizer (OPS) model 3330 and an aethalometer Magee AE33, respectively. Furthermore, to assess the emissions of BrC from smoldering combustion processes, the AAE was estimated. Finally, two collocated PM LCS, Sensirion SPS30, were used together with the reference instrument for both the long-term analysis and transient events. SPS30 sensors were chosen for their superior performance compared to others [24, 48, 49], their low cost, and compact size which make them easily adaptable for use in indoor environments with limited spaces. To our knowledge, this is the first long-term study to examine the precision, accuracy, and durability of SPS30 sensors for indoor use.

2. Description of the Site

The measurement site is the Potenza research area located in South Italy (Tito Scalo, 40.60° N , 15.72° E , 750 m a.s.l.) in a small industrial zone, placed in a large rural area surrounded by Apennine Mountains and near a few small plants, a busy main road, and a shopping mall. The research area hosts a complex building (Figure 1) with three institutes of the National Research Council including laboratories, offices, a library, a data center, a conference room, and a guesthouse. About 100 workers are expected to carry out their activities daily in the area.

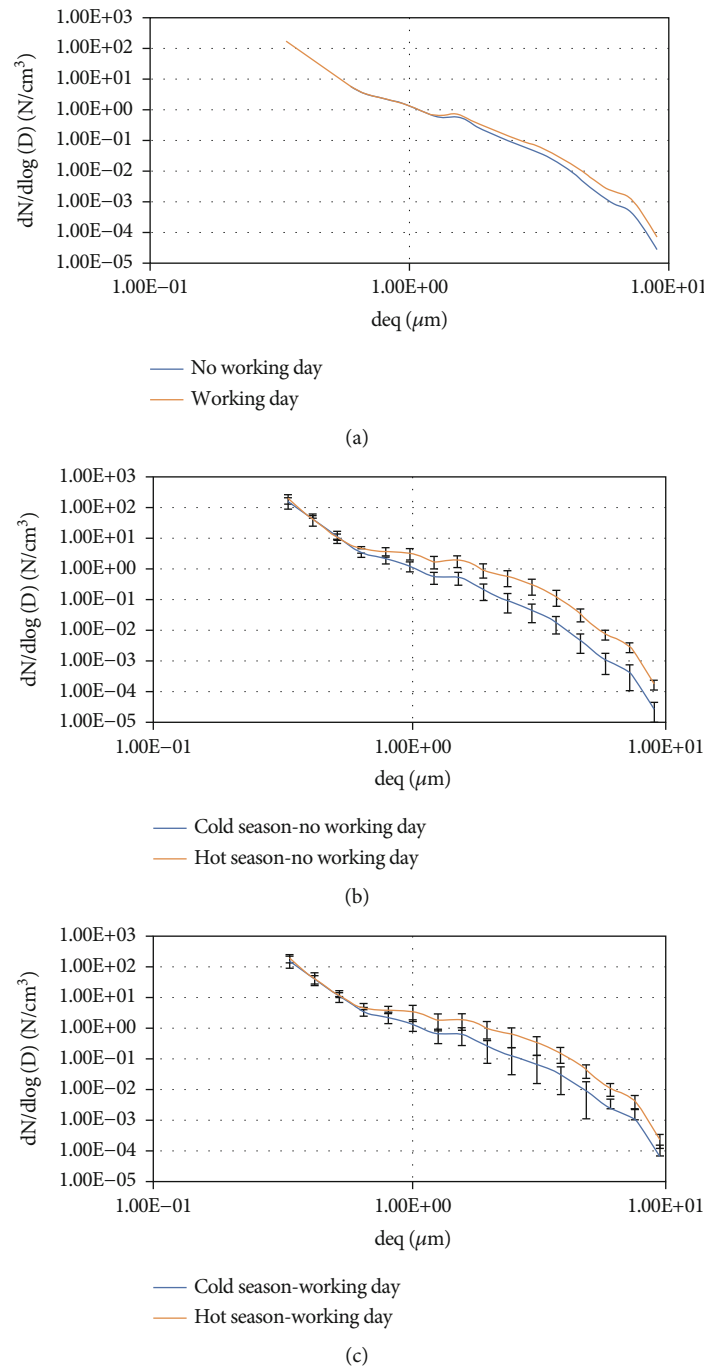


FIGURE 2: (a) Mean number size distribution for working and nonworking days for the whole dataset. (b, c) Mean number size distribution for working and nonworking days and for hot and cold seasons. Vertical bars represent standard deviations. For color images, please refer to the online version of the article.

The complex building consists of three two-level edifices (edifices 1-3 in Figure 1) hosting laboratories (ground floor) and offices (first floor), a two-level edifice (edifice 4 in Figure 1) hosting offices and a conference room (ground floor) and offices and a library (first floor), and a three-level edifice hosting common facilities (ground floor), offices (first floor), and a guesthouse (third floor). The five edifices are interconnected, whereas edifice 6, devoted to plant engineering, is an independent building. Measurements were conducted in a

laboratory/office located on the ground floor of edifice 1 (Figure 1). During working hours (8:30 a.m.-17:00 p.m. local time (LT), approximately from Monday to Friday), one or two employees are present in the room.

Apart from the infiltration (building envelop characteristics) and penetration (opening and closing the door at 8-9 a.m. and 4-5 p.m. local time (LT)) of outdoor particles, possible indoor sources, related to the activities in the lab/office room, include particle resuspension due to people moving and operation of

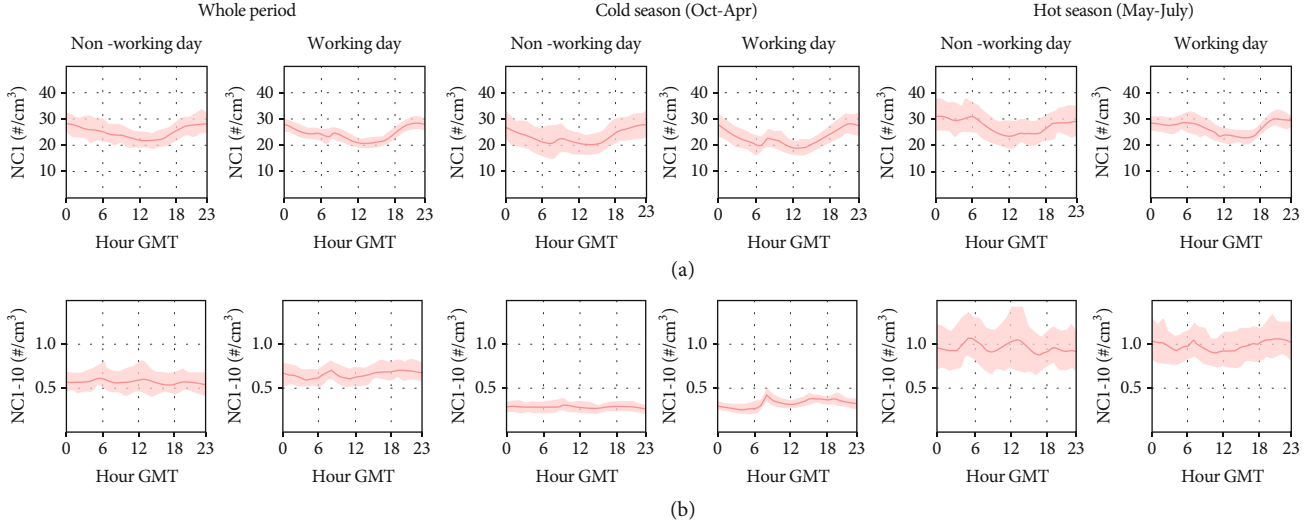


FIGURE 3: (a) Diel (working and nonworking) cycles of NC_1 fraction for the whole period, cold, and hot season. (b) The same for NC_{1-10} fraction.

the mechanical ventilation system from approximately 8-9 a.m. to 4-5 p.m. (LT), during the cold season.

An exhaustive characterization of the outdoor sources of aerosols at the site, as suggested by previous works [50–53], classified the site as semirural, often affected by Saharan dust intrusions each year, and with the influence of vehicular traffic emissions from the close main road.

3. Materials and Methods

3.1. Instruments. The indoor aerosol characterization was obtained by collecting multi-instrumental data on a long-term basis. The instruments used were a TSI OPS 3330 to obtain number particle size distributions in the size range $0.3\text{--}10\text{ }\mu\text{m}$ (16 channels) and an aethalometer Magee AE33 to measure the eBC concentrations and estimate AAE. Further details on the instrumentation can be found in [54]. In addition, four experiments were performed to characterize aerosol transient emissions from some common indoor sources at the research area such as incense, electric and traditional cigarettes, and HNB products. During these short-term experiments, a TSI versatile water-based condensation optical particle (V-WCPC) model 3789 was used to determine the number concentrations (NC) of UFP and fine particles down to 2.5 nm in diameter with 1 min time resolution [55].

The testing of two PM LCS Sensirion model SPS30 (units 5F65C and BB687) was carried out both on a long-term basis and for the four transient events using the OPS as a reference instrument. The SPS30 sensor utilizes a measurement technology based on laser scattering and provides particle size distribution in four bins in the range $0.3\text{--}10\text{ }\mu\text{m}$, as well as PM_1 , $PM_{2.5}$, PM_4 , and PM_{10} mass concentrations. The sample airflow is generated by means of a fan, and the sampling time is 1 s . The SPS30s were calibrated by the manufacturer for $PM_{2.5}$ number size distribution using a TSI OPS model 3330. Additionally, SPS30 has a contamination-resistance technology that prevents the sensor's optical components from contamination because of particle accumulation

[56]. The Sensirion SPS30 is equipped with an automatic fan cleaning procedure which ensures the sensor's accuracy even during monitoring in a high polluted environment [57].

It also has an associated viewer software for data logging, visualization of real-time data, setting of the averaging time of sensor outputs, and selection of the auto cleaning interval if auto cleaning is enabled. However, due to the lack of internal storage, the SPS30 must be connected to a computer to gather data.

Owing to the very low number count density in PM_4 and PM_{10} fractions, attention should be paid when considering coarse particle detection as suggested by the manufacturer [56]. The limited reliability of SPS30 in measuring large particle concentrations was verified in [24, 48, 49]. In the same works, a good performance of SPS30 in revealing fine particle was assessed.

Some tests were carried out to choose the suitable averaging time of sensor outputs, which was set to 100 s (see Figure S1 of the Supplementary material).

3.2. Experimental Set-Up and Dataset Description. All the measurements were carried out in a laboratory/office with a surface area of approximately 40 m^2 placed on the ground floor of edifice 1 (Figure 1). It has natural ventilation (doors and windows) and a mechanical ventilation system which is used in wintertime for heating. No filtration system is present in the mechanical ventilation system. The instruments were placed on a table (90 cm high) near the door, opposite the desk where two employees usually work (Figure 1).

During the short-term experiments, a window and the door of the laboratory/office were left open. All sources were placed at approximately 1.5 m from the instrumentation.

The long-term dataset, lasting from October 2021 to July 2022, included hourly and daily averaged number size distributions from OPS data and the two Sensirion SPS30 units, respectively, as well as hourly and daily averaged eBC mass concentration and AAE values from aethalometer measurements.

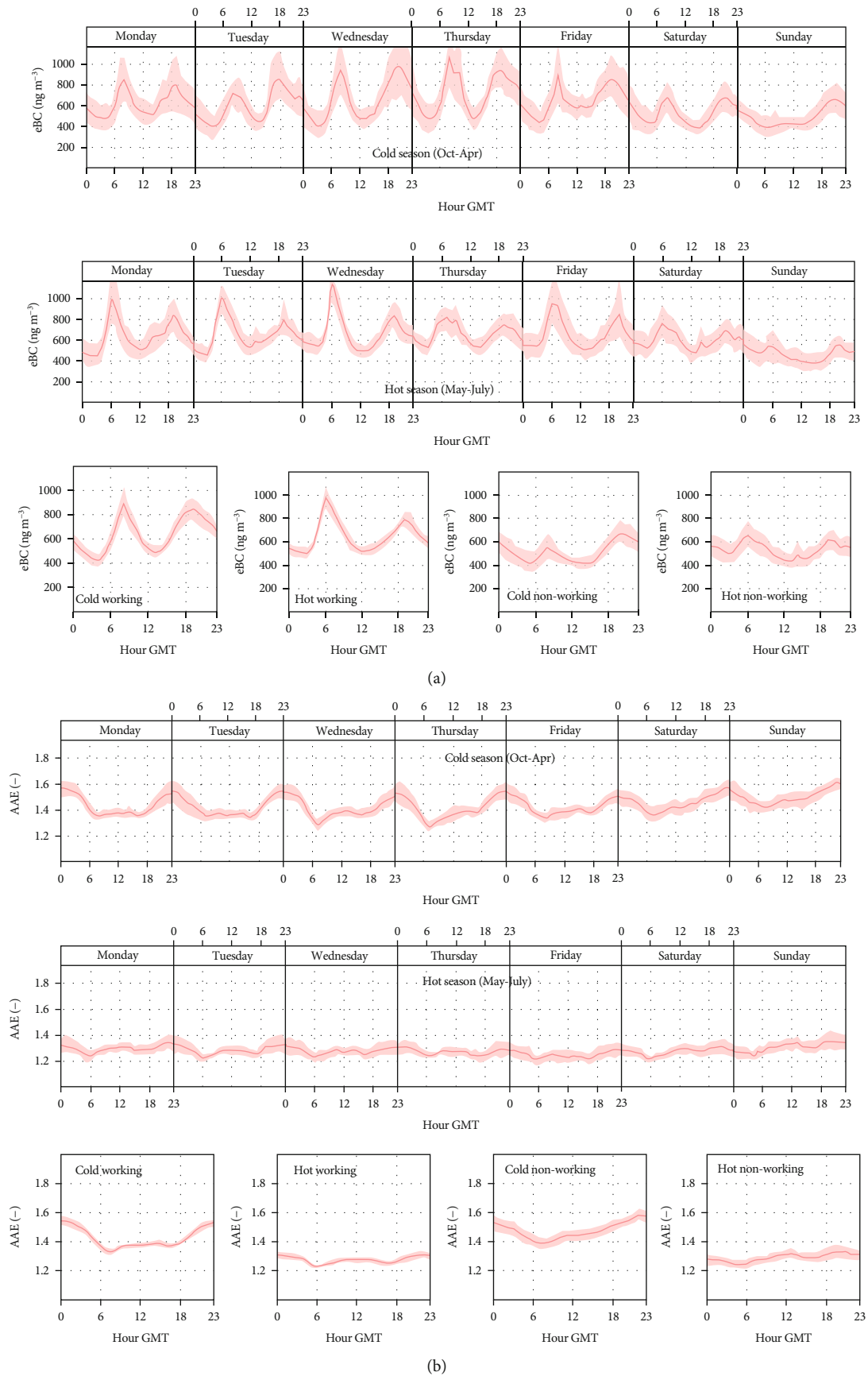


FIGURE 4: (a) Weekly and diel (working and nonworking) cycles of eBC for the cold and hot season. (b) The same for AAE.

As regards the four transient pollution events, data from all instruments were collected on March 1, 2, 4, and 8, 2022. 1 min CPC and aethalometer data were smoothed in a 5 min moving average and compared to 5 min OPS measures. These data were excluded from the long-term dataset analysis.

4. Results and Discussion

4.1. Long-Term Dataset

4.1.1. OPS Size Distribution. OPS mean size distributions were calculated separately for working and nonworking days and for the cold (October–April) and hot (May–July) seasons, as shown in Figure 2. Working and nonworking days' size distributions show a similar shape over the entire dataset, with a mode at $1.56\ \mu\text{m}$ which can be associated to particle resuspension due to the traffic source, as previously assessed in [54]. Working days are characterized by a slightly enhanced contribution of coarse particles, becoming more pronounced during the hot season.

To compare the fine and coarse contribution to number concentrations, OPS data were grouped into two fractions, NC_1 including particles with diameter from 0.3 to $1\ \mu\text{m}$ and NC_{1-10} for particles with diameter from 1 to $10\ \mu\text{m}$. Looking at the diel cycle of the NC_1 fraction shown in Figure 3(a), for the whole period, an increased concentration is found during nighttime. This pattern is partly driven by the cold season behavior owing to the biomass burning from domestic heating source, whereas during the hot season, a flatter pattern is obtained. The boundary-layer dynamics could have contributed to these trends [58].

Despite the high standard deviation of NC_{1-10} diel cycles, especially for hot season data, a clear increase of concentration during this season can be inferred. This can probably be due to the semirural nature of the site, the reduction of rain events, and to the higher frequency of long-range dust advection episodes registered during the hot season, as detailed in Section 4.1.3. Moreover, a peak during the morning is well distinguishable when working days are considered, which is likely associated with the resuspension of coarse particles from the traffic sources. For both NC_1 and NC_{1-10} fractions, a higher variability characterizes the hot season data.

4.1.2. eBC and AAE. Looking at Figure 4, a clear pattern for eBC diel cycles is obtained, indicating the traffic from outdoor as the main source of indoor eBC. In [53], outdoor eBC measurements in this area highlighted the two-peak behavior of carbonaceous particle concentration, typical of traffic sources. In their work, the authors concluded that the outdoor eBC at the research building area was strongly influenced by the presence of a main busy arterial (about 20,000 vehicles per day [59]) passing at about 1 km from the site. The two peaks' behavior shows seasonal features in terms of morning/evening peak intensity ratio. In fact, during the cold season, the morning and evening peaks show similar intensities though the evening peak is broader. Conversely, during the hot season, the morning peak prevails over the evening peak. This can be partly attributed to a

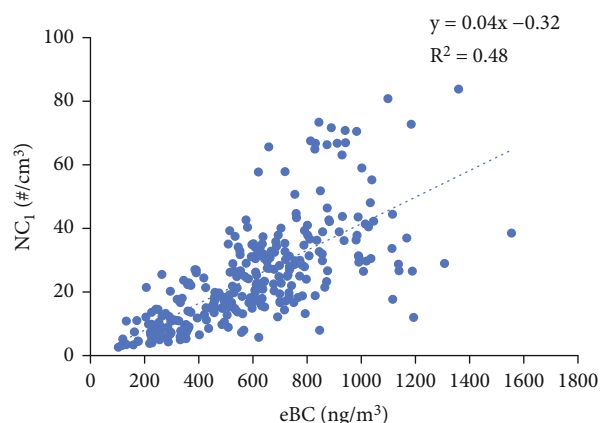


FIGURE 5: Scatterplot of daily mean NC_1 vs. eBC data over the whole dataset.

different dynamic of the boundary layer between the two periods, as found in [58] for a similar site.

As expected, a nighttime increase in AAE is visible during the cold season when higher values are typically found compared to the warm season. This is mainly caused by the biomass burning for domestic heating [53]. In general, AAE values are higher during weekends compared to working days, likely due to agricultural activities [54]. During the cold season, AAE values are slightly higher during weekends than on working days, as biomass burning for domestic heating is likely used more frequently than on weekdays due to people spending more of their time at home.

4.1.3. Influence of Outdoor Sources. From the results obtained, the influence of traffic and domestic heating as outdoor sources of indoor fine fraction abundance can be inferred. A confirmation of the influence of the traffic can be derived by the scatterplot between NC_1 and eBC over the long-term dataset, as shown in Figure 5. The correlation coefficient of 0.48 indicates that eBC has an influence on NC_1 , although it is not the only influencing factor.

The measurement site has semirural nature, with soil erosion by wind, and there is dust resuspension; thus, the outdoor particle penetration is expected to have an influence on the indoor coarse fraction. This was verified by comparing the time series of daily indoor NC_{1-10} and PM_{10} measured at a monitoring station close to the measurement site and managed by the Regional Agency for the Environment of Basilicata (ARPAB) resulting in a R^2 of 0.63 as shown in Figure 6. The comparison also indicates the long-range transport of desert dust and sea salt as an additional outdoor source of coarse particles as shown in Figure 6. In Figure S2 of the Supplementary Material, NAAPS maps (https://www.nrlmry.navy.mil/aerosol/index_frame.html) and Hysplit back-trajectories (<https://www.ready.noaa.gov/HYSPLIT.php>), supporting this finding, can be found.

4.2. Emission Study of Selected Sources. The tests were carried out from March 1 to March 8, 2022, to examine eBC concentrations, AAE parameter, and number size distributions of aerosols originating from some indoor sources commonly

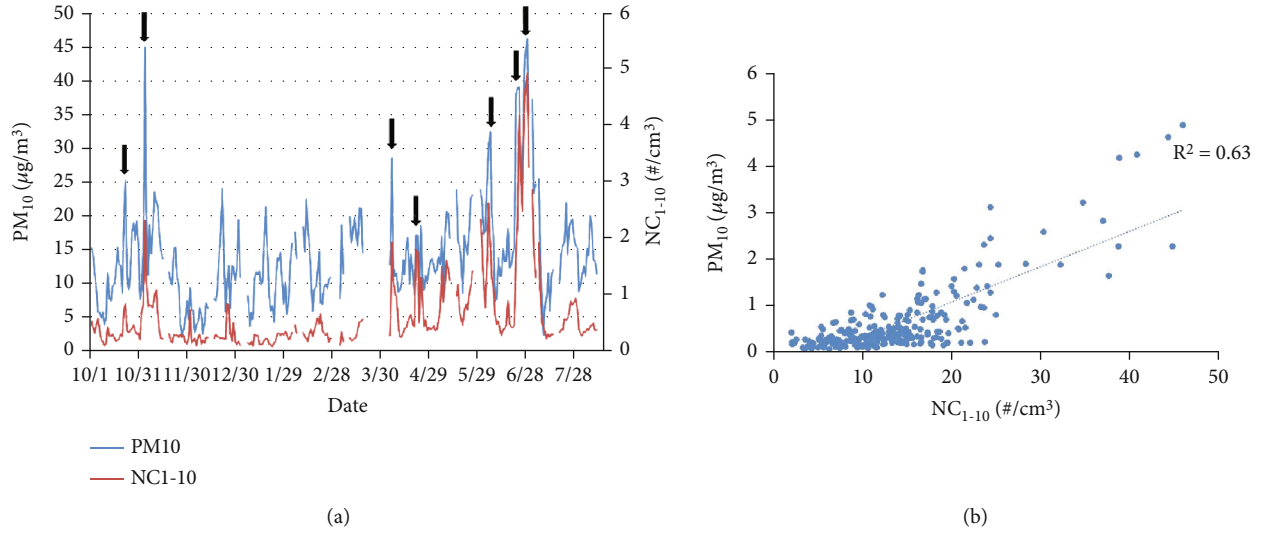


FIGURE 6: (a) Temporal trend of daily mean PM₁₀ and NC₁₋₁₀ and (b) corresponding scatterplot. Black arrows indicate Saharan dust advection episodes. For color images, please refer to the online version of the article.

TABLE 1: List and duration of the tests carried out for the four indoor sources: incense, electric and traditional cigarettes, and heat-not-burn (HNB) products.

| Event | Date | Duration | |
|------------------------|---------|------------|------------|
| Incense burning | March 1 | 20 minutes | |
| E-cig | March 2 | Session 1 | 10 minutes |
| | | Session 2 | 6 minutes |
| | | Session 3 | 4 minutes |
| Conventional cigarette | March 4 | Session 1 | 7 minutes |
| | | Session 2 | 5 minutes |
| HNB device | March 8 | Session 1 | 2 minutes |
| | | Session 2 | 4 minutes |
| | | Session 3 | 4 minutes |

used at the research area. In Table 1, details of the experiments are listed, whereas the temporal variations of the parameters are plotted in the graphs of Figure 7.

4.2.1. Incense. The incense test consisted of burning an incense cone from 2.27 p.m. (20-minute duration) on March 1. UFP concentration shows a broad peak starting at the ignition of the incense cone and decaying at a few minutes after the cone's extinguishing, as reported in Figure 7. The peak concentrations ranged from about $5000 \#/ \text{cm}^3$ to a maximum of $66000 \#/ \text{cm}^3$, in accordance with the UFP incense peak concentrations reported in [60]. The temporal trend of total number particle concentration peak is similar to those described in [16, 61] though they reported maximum concentration 20- to 30-fold higher than the background, whereas in our case, it was found 10-fold higher. This discrepancy could be attributed to the different burning times of incense, varying room conditions (door closed), and experimental settings. The NC₁ fraction shows a double peak: the first occurring a few minutes after the ignition,

when the UFP peak starts growing, and the second during the cone burning, highlighting the emission of fine particles. The eBC concentration follows NC₁, rather than UFP number concentrations. For comparison, some studies such as those of [62, 63] have investigated brown carbon content in relation to smoldering biomass combustion using incense as a surrogate for stronger absorption at shorter wavelengths. The authors calculated the AAE parameter as the negative slope of the absorption coefficient versus wavelengths (355, 405, 532, 870, and 1047 nm) in a log-log plot obtaining a value of 4.53. High values of AAE (>4) were also found in [62], where the couples of wavelengths 405-532 nm and 532-781 nm were considered for AAE calculation. In this work, incense-related AAE was 2.72, the highest among all other sources tested.

4.2.2. E-Cigarette. The test with the e-cig consisted of three vaping sessions performed by the same volunteer. The e-cigarette was filled with e-liquid containing 2.2 mg mL^{-1} of nicotine. It was lit for ten minutes from 2:30 p.m. on March 2, then lit again at 3:36 p.m., and turned off at 3:42 p.m., and finally, it was vaped from 4:34 p.m. to 4:38 p.m. As regards the UFP particles, comparable number concentrations were found in [17], who used similar experimental set-up for e-cig testing. However, it is worth noting that the types of kit and e-liquid used may cause substantial variability in e-cig emissions [19, 64]. Moreover, even in the absence of combustion processes during vaping, the eBC peaks are distinguishable in the graphs of Figure 7, with a maximum after the third vaping session. This could be due to the burning of residual incrustation on the coil promoted by the high temperatures reached ($>1000^\circ\text{C}$) when no saturation with e-liquid occurs in the tank [65].

4.2.3. Conventional Cigarettes. The test with the traditional cigarette consisted of two smoking sessions, performed by the same smoker, lasting seven and five minutes, respectively,

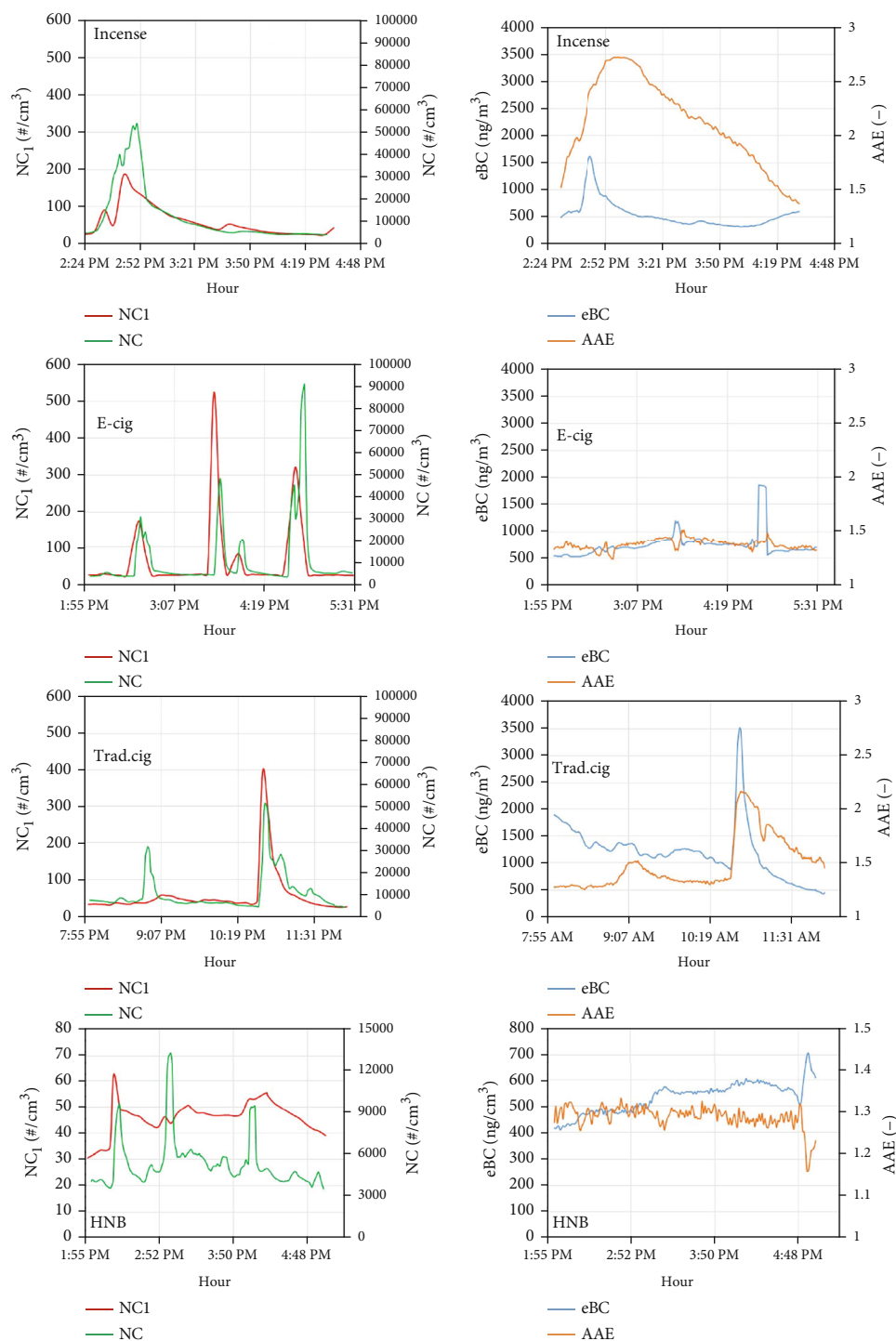


FIGURE 7: Temporal variations of NC_1 , NC, eBC, and AAE data during the five tests. Please note that HNB source was plotted with a different y-axis extension to enable cleaner visualization. For color images, please refer to the online version of the article.

from 8:48 a.m. to 8:55 a.m. and from 10:36 a.m. to 10:41 a.m. on March 4.

UFP concentration showed two peaks, one at the end of the first smoking session and the other, broader and more intense than the first, a few minutes after the end of the second smoking session, as shown in Figure 7. The eBC concentration increased simultaneously with the second UFP peak. A similar behavior was also seen for AAE and

NC_1 although there was a slight growth visible a few minutes after the first cigarette as well. Together with incense, traditional cigarettes were found to be the strongest emitters of BrC according to AAE values in Figure 7, but different dynamics can be identified. In the case of cigarettes, a narrow peak of AAE values is visible, similar to those of eBC, NC, and NC_1 , whereas for incense, AAE values decay more slowly compared to eBC and NC_1 . This difference

TABLE 2: Contributions of different sources to NC₁, NC, eBC, and AAE increase, measured during tests.

| Parameter | Contribution in decreasing order |
|--------------------------|------------------------------------|
| NC (CPC) | E-cig > incense = trad. cig. > HNB |
| NC ₁ (OPS) | E-cig > trad. cig. > incense > HNB |
| NC ₁₋₁₀ (OPS) | E-cig > trad. cig. > HNB > incense |
| eBC | Trad. cig. > incense > e-cig > HNB |
| AAE | Incense > trad. cig > e-cig > HNB |

can be attributed to the presence of primary absorbing particles emitted during cigarette burning compared to incense, when a secondary origin for BrC can be hypothesized. The delay of NC peak with respect to NC₁ peak in the case of incense further supports this hypothesis.

4.2.4. Heat-Not-Burn (HNB) Product. The HNB devices heat the tobacco stick without burning it. For the experiment with HBN, the same device was used during three sessions, with one tobacco stick smoked, for each session, by the same volunteer. The HNB was lit at 1:15 p.m. on March 8 with a vaping time of two minutes, then it was vaped for four minutes from 1:55 p.m., and finally it was lit at 2:57 p.m. and turned off at 3:01 p.m.

UFP concentration shows three peaks, each a few minutes after the lighting of the HNB. Three broader peaks were found for NC₁ but shifted compared with CPC ones as illustrated in Figure 7. The temporal trends of eBC and AAE seem to be unaffected by HNB emissions, suggesting no production of absorbing particles from this source as found in [19]. In their experiment, carried out inside a traveling car, traditional cigarette, e-cig, and HNB BC emissions were compared, resulting in HNB as the only smoking device with no spike in BC concentration. Looking at Figure 7, significantly lower concentrations of both UFP and fine particles were found for HNB compared to e-cig and traditional cigarettes in accordance with the recent literature on the matter [66–71]. However, comparing, for example, the similar experiments carried out by [67, 68], where emissions from two HNB devices with different sticks were analyzed, an elevated variability in particle emission is evident. For this reason, the results obtained for the HNB device used in the present work may not be directly comparable to other brands or of different configurations of the same product.

4.2.5. Source Comparison. A comparison among different source emissions was carried out as summarized in Table 2.

As regards UFP, the most intense source is e-cig, followed by incense and traditional cigarettes, demonstrating a similar impact, and lastly HNB. This confirms the findings of [26] about the relevance of e-cig source in the production of UFP particles. Figure 7, shows how e-cig and HNB emissions exhibit the quickest decay in agreement with the results reported in [19]. In terms of NC₁ behavior, the most intense source was e-cig, followed by traditional cigarette and incense then HNB. Among the four sources, e-cig showed the most intense peaks in fraction NC₁₋₁₀ in

agreement with the findings of [72], which used an aerodynamic particle sizer (APS) in conjunction with a Scanning Mobility Particle Sizer (SMPS) to detect a mode at approximately 1000 nm. Similarly, the recent research by [73] also made note of considerable emissions of 1–2 μm aerosols. It is possible that the release of metal and silicates from the coil and tank, as mentioned in previous studies [65, 74–76], contributes to this phenomenon. According to [65], metal emission can be favored by the degradation of the coil due to the high temperatures reached (>1000°C) when the wick is not saturated with e-liquid. The degradation of the coil, visible for the e-cig used in the present experiment, corroborates this hypothesis. As far as combustion-related emissions are concerned, the most intense eBC emitter is the traditional cigarette, followed by incense and e-cig (similar) and HNB, whereas incense and traditional cigarettes show higher AAE values, followed by e-cig and HNB. In Figure 8, the temporal trends of particle size distribution for the four experiments are shown. The plots highlight the emission behavior of the short-duration sources with an increase of particles in the range 0.3–1 μm for all sources; in some cases, super micron particles were also emitted.

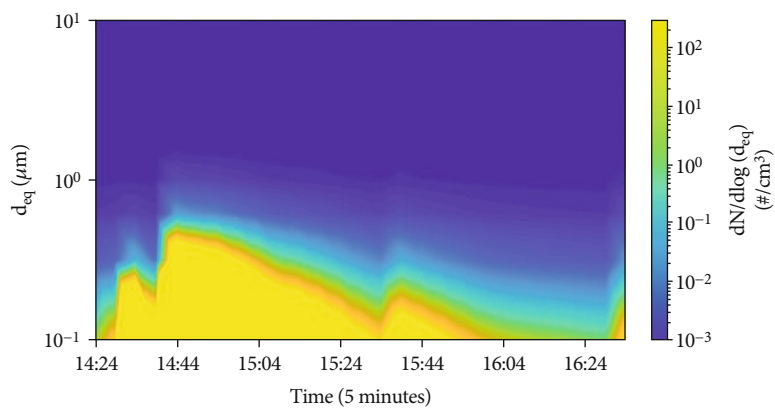
These fractions were poorly characterized in the literature [6, 16, 72, 73], since generally FMPS or SMPS were used for similar experiments. However, in real-life conditions, the coagulation and condensation processes can lead to the formation of coarser particles, which can increase the amount of aerosol deposited in the upper respiratory tract, compared to UFP.

4.3. SPS30 Performance Evaluation. To test the performance of SPS30 sensors, the number concentrations were calculated by aggregating the data into two size intervals NC₁ and NC₁₋₁₀, as previously done for OPS data. However, following [49], the analysis of the results was carried out for the NC₁ fraction only, owing to the low reliability of SPS30 estimates of number concentration in the range 1–10 μm .

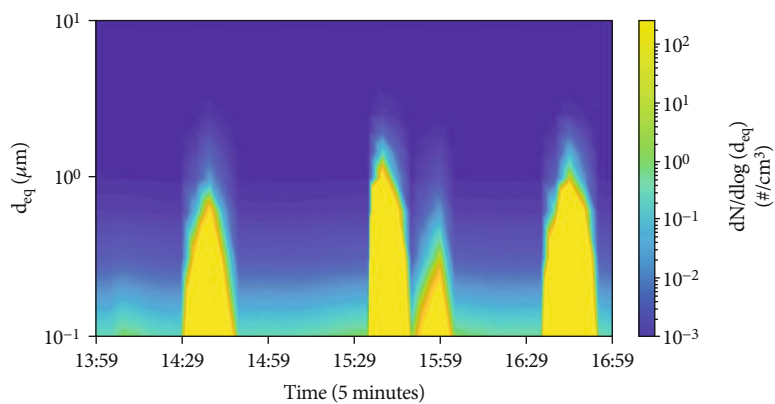
SPS30s were evaluated both for precision, by intramodel comparison, and accuracy, by testing them against the OPS on a 1 h and 24 h time basis. Moreover, the long-term stability was checked. Coefficient of determination (R^2) and slope from a linear fit, Spearman's coefficient (ρ), root mean square error (RMSE), and coefficient of variation (CV) were used as evaluation metrics [37, 40, 77–79]. The assessment of CV was considered for precision evaluation only, as a metric to compare the two units of the SPS30 sensor model.

4.3.1. Long-Term Dataset. Precision and accuracy of SPS30s were first evaluated on a long-term basis. Results are shown in Table 3 for NC₁ fraction. As far as drift is concerned, the temporal trend of the difference between sensor and reference data was analyzed over the entire dataset.

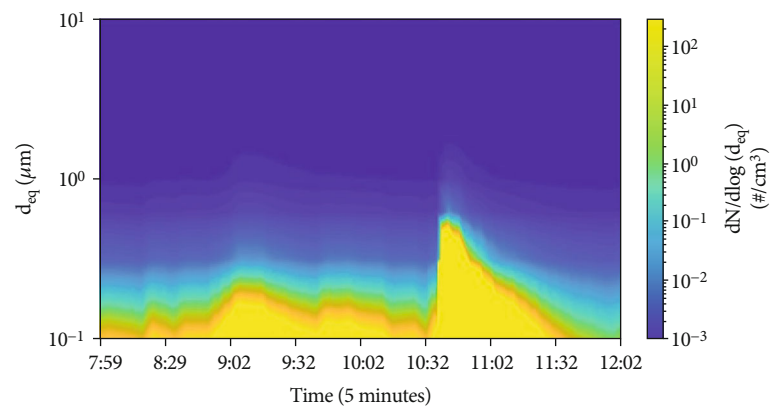
The values of both R^2 and slope fall in the range indicated in [40] as satisfactory to infer a good sensor performance. This translates in the capability of SPS30 to follow the variations of number concentrations as measured by OPS in the range 0.3–1 μm , as confirmed by the time series of daily values plotted in Figure 9.



(a)



(b)



(c)

FIGURE 8: Continued.

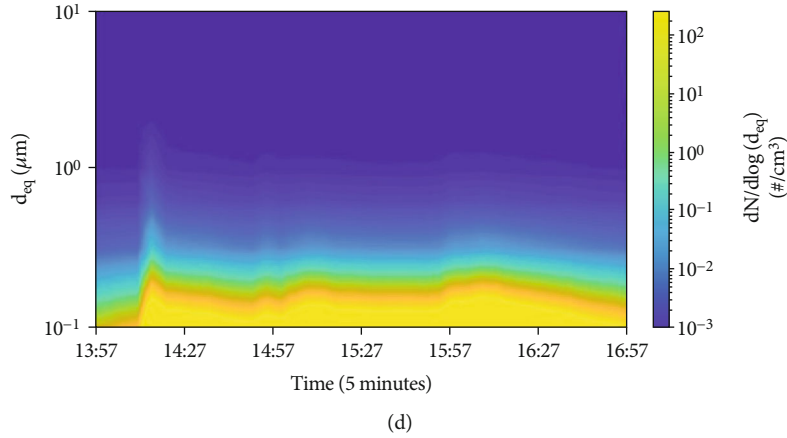


FIGURE 8: OPS particle number size distributions in the range 0.3–10 μm for (a) incense, (b) e-cig, (c) trad cigarette, and (d) HNB. For color images, please refer to the online version of the article.

TABLE 3: Sensor performance for NC_1 fraction measured by the two SPS30 units. Both precision and accuracy evaluation metrics include R^2 , the slope, and the Spearman coefficient (ρ). RMSE was calculated only for SPS30 and OPS comparisons, while the CV was determined only for intramodel comparison. Statistical parameters were calculated both on a 1 h and 24 h basis.

| NC_1 | Precision | | Accuracy | | | |
|------------------|-----------------|------|----------------------------|----------------------------|----------------------------|----------------------------|
| | 5F65C vs. BB687 | | OPS vs. 5F65C | | OPS vs. BB687 | |
| Temporal average | 1 h | 24 h | 1 h | 24 h | 1 h | 24 h |
| R^2 | 0.99 | 0.99 | 0.87 | 0.89 | 0.88 | 0.90 |
| Slope | 0.98 | 0.97 | 1.17 | 1.16 | 1.16 | 1.14 |
| ρ | 0.99 | 0.99 | 0.93 | 0.94 | 0.93 | 0.94 |
| RMSE | / | / | 13.11 ($\#/\text{cm}^3$) | 12.2 5($\#/\text{cm}^3$) | 12.72 ($\#/\text{cm}^3$) | 11.81 ($\#/\text{cm}^3$) |
| CV (%) | 2.97 | 2.21 | / | / | / | / |

The high linearity ($0.87 < R^2 < 0.90$) found between the number concentrations measured by SPS30s and OPS (Figure 9) is consistent with [80]. Sousan et al. [80] found a high correlation between the SPS30 sensors and the reference instrument for mass concentration of three types of laboratory-generated aerosol in both environmental and occupational setting conditions.

Considering the slope of the regression line between the two SPS30 units and OPS, values higher than one indicate an overestimation of the number concentration. Similar results were obtained in the South Coast Air Quality Management District (SCAQMD, USA) field test, where mass concentrations from three SPS30 units were compared to those obtained by three reference monitors in outdoor conditions [81]. Additionally, a response comparable to this was registered in [57] when comparing SPS30 and aerodynamic particle sizer (APS) number concentrations for laboratory-generated aerosols.

To investigate the SPS30 sensor response to distinct levels of particle loading, the Pearson coefficient (r) between SPS30 and OPS NC_1 hourly data was calculated separately for each quartile of OPS number concentrations. Results are illustrated in Figure 10 showing a better performance of both SPS30 sensors for increasing aerosol number concentration, in agreement with the findings of [40, 79] in the case of mass concentrations.

The low values of CV in Table 2 highlight a high precision for collocated SPS30 sensors in accordance with [57], where SPS30 was more precise than Plantower PMS5003 in measuring laboratory-generated ammonium sulfate, nebulized Arizona road dust, NIST Urban PM, or oil mist.

To evaluate the possible drift in sensor outputs over time, the temporal pattern of the absolute value of the difference between the sensor and the reference daily number concentration was calculated, as reported in Figure 11. A slightly increasing trend is visible indicating the effect of prolonged recording time on sensor measures [25].

4.3.2. Transient Events. Measurements of number concentrations by means of the two SPS30 sensors were carried out during the tests with the selected sources described in Section 4.2, allowing examination of their efficacy in detecting real short-lasting pollution events in an indoor environment. SPS30 data were time paired with the 5 min OPS measures for comparison, and the corresponding time series are shown in Figure 12. R^2 coefficients for both sensor units were calculated and reported in the upper corner of the graph. As it is possible to see, SPS30s succeeded in the detection of all events with varying accuracy: a good agreement ($R^2 \geq 0.6$) was obtained in the case of incense, traditional cigarette, and HNB, whereas a worse result was found for

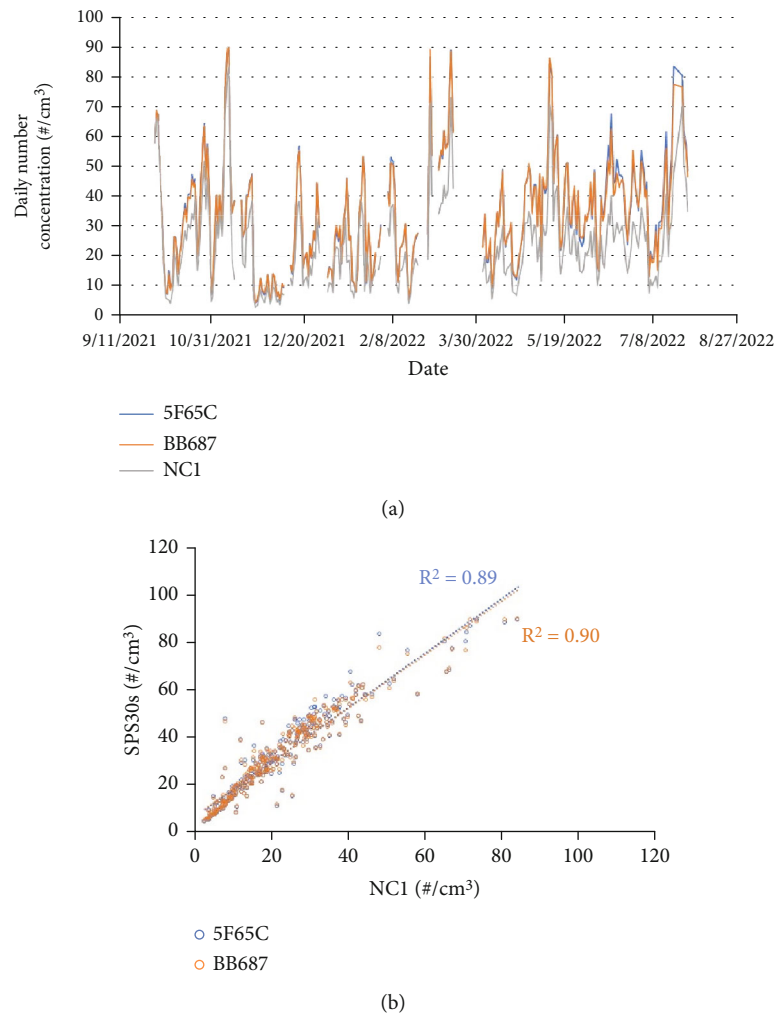


FIGURE 9: (a) Temporal trend of daily mean NC_1 measured by the OPS and the two SPS30s and (b) corresponding scatterplots. For color images, please refer to the online version of the article.

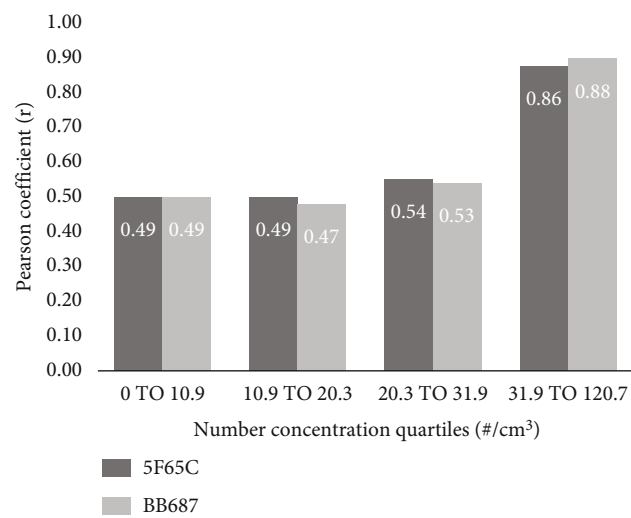


FIGURE 10: The Pearson coefficient for hourly NC_1 from SPS30 sensors against hourly NC_1 from OPS, calculated for the four quartiles of OPS concentration.

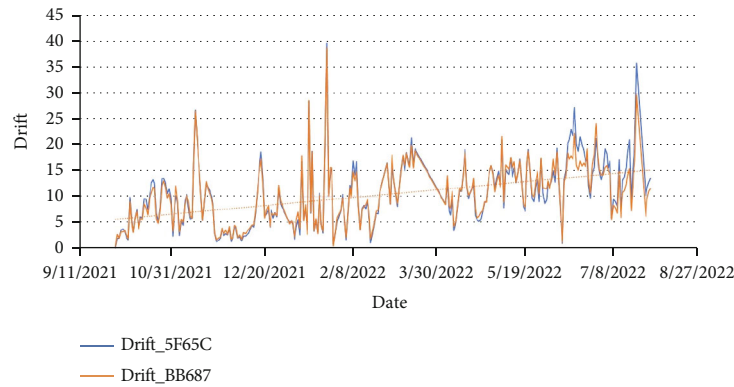


FIGURE 11: Time variation of the absolute value of the difference between daily mean NC_1 measured by the OPS and the two SPS30s. For color images, please refer to the online version of the article.

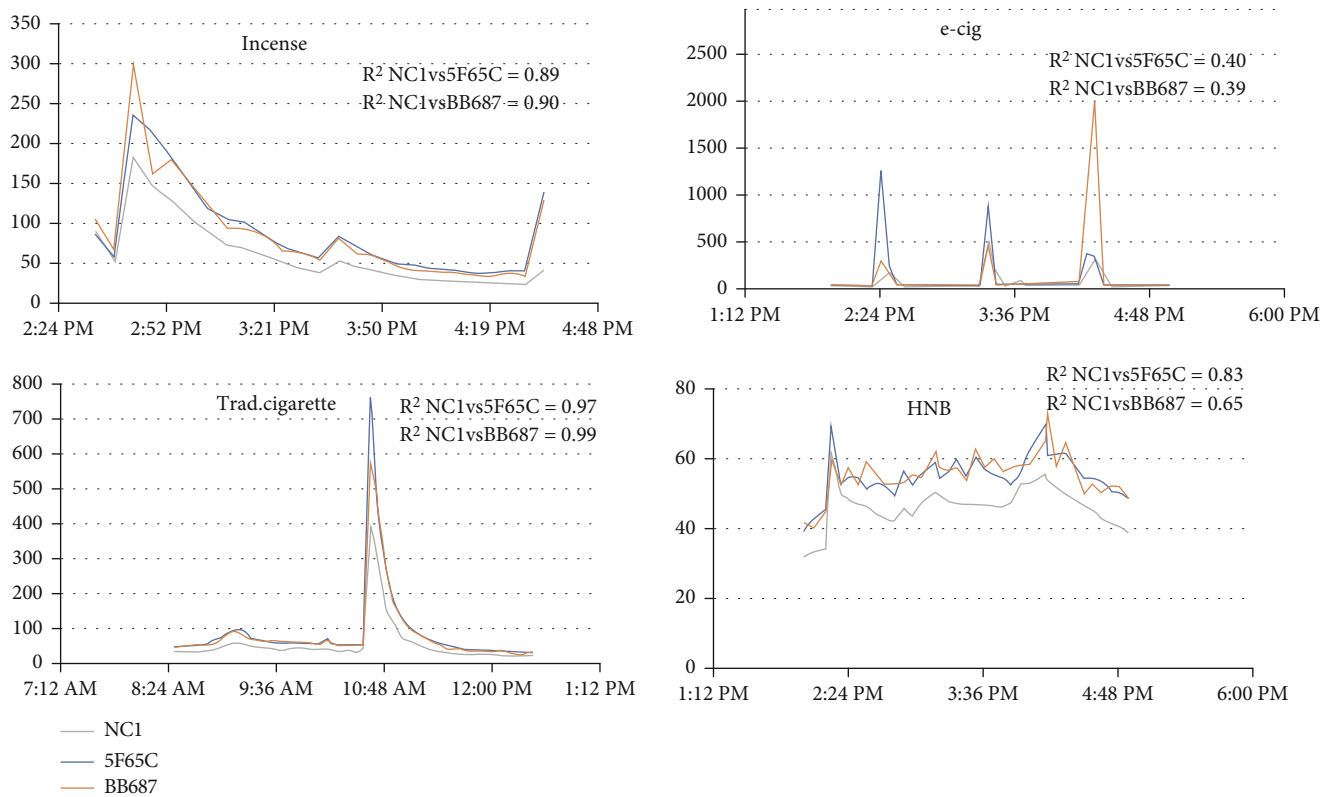


FIGURE 12: Temporal trend of NC_1 measured by the OPS and the two SPS30s during the four transient pollution events. Please note that different y -axis extensions were used to enable cleaner visualization. For color images, please refer to the online version of the article.

e-cig. This could be related to the duration of the emission peaks of the different sources. In fact, among the sources, e-cig peaks show shorter temporal extents with faster changes in number concentration.

5. Limitations and Further Research Directions

In the present work, only a single model of each smoking device (e-cig, traditional cigarette, and HNB) was used as short-duration high-emission source in the experiments. Given the large variety of models and technologies available, especially in the new-generation smoking devices, the results

obtained here may not account for the variability of emissions of such sources.

The experiments were conducted in real-life conditions, and an extensive analysis of the influence of parameters such as temperature or humidity on LCS performances has not been carried out yet. The development of a low-cost network for indoor air quality control based on LCS represents a further research direction. To this aim, the performance evaluation of LCS under different ambient parameters will be assessed in indoor environments. Moreover, the potentiality of new-generation LCS for UFP and nanoparticles detection will be studied.

6. Conclusions

A long-term indoor campaign was carried out at a research area building located in a semirural site in South Italy to characterize aerosol number size distributions and carbonaceous particles. Short-term intense emission events common to the research area were simulated and included in the analysis. Moreover, the performances of two PM LCS, Sensirion SPS30, were evaluated comparing LCS data with the number size distributions obtained by the reference instrument. The main results are summarized in the following:

- (i) The analysis of the long-term dataset suggests that infiltration and penetration of outdoor particles strongly influence the number particle concentration in both fine and coarse fractions; traffic (BC and resuspended dust) and domestic heating (BrC) are the main sources of indoor particles from outdoor
- (ii) The short-term experiments with the four indoor sources showed that HNB has the smallest impact on particulate loading; e-cig emits particles with dimensions spanning from ultrafine to coarse, probably due to the release of metal and silicate by the heating coil degradation
- (iii) The transformation processes modify the particle size distribution after emission, as highlighted during the experiments; this could influence penetration and deposition rate in the human respiratory system
- (iv) Concerning the comparison between OPS and LCS, a good agreement for both long-term and short-term experiments is observed, along with a slight degradation of the LCS long-term performance

The results obtained suggest best practices to adopt for the health of workers, especially when high emission sources are present. Moreover, the comparison of SPS30 PM LCS and OPS TSI 3330 data clearly demonstrates their feasibility in supporting indoor air quality evaluation on both the long-term basis and for transient events.

Data Availability

The authors can make data available on request. The corresponding author, Mariarosaria Calvello, should be contacted to request the data (mariarosaria.calvello@imaa.cnr.it).

Conflicts of Interest

The authors declare that they have no known competing financial interests or personal relationships that could have appeared to influence the work reported in this paper.

Authors' Contributions

Mariarosaria Calvello was responsible for the conceptualization, investigation, and formal analysis, wrote the original draft, and wrote, reviewed, and edited the manuscript. Francesca Agresti was responsible for the data curation,

investigation, and formal analysis. Francesco Esposito was responsible for the data curation, formal analysis, and investigation. Giulia Pavese was responsible for the conceptualization, investigation, funding acquisition, project administration, and supervision and wrote, reviewed, and edited the manuscript. All listed authors made a significant scientific contribution to the research in the manuscript, approved its claims, and agreed to be an author.

Acknowledgments

The authors are grateful to Luchsinger s.r.l and Dr. Somaschi for borrowing the TSI V-WCPC model 3789. The NOAA Air Resources Laboratory (ARL) for HYSPLIT model and the NRL/Monterey Aerosol Page for NAAPS maps are acknowledged. This work is partly supported by the PhD project "Innovative technologies for the quality of living environment in manufacturing systems" in the framework of cooperation between the Italian National Council of Research and the Italian Main Association of Manufacturing and Service Companies.

Supplementary Materials

Some tests were carried out to choose the suitable averaging time of sensor output signals, which was set to 100 s, as a satisfactory compromise between time resolution and noise/signal ratio. Figure S1: temporal trends of BB687 unit signals acquired over (a) 1 s, (b) 10 s, (c) 100 s, and (d) 1000 s. Maps NAAPS and Hysplit back-trajectories were shown for two of the days affected by Saharan dust transport during the measurement campaign, as representative of the intrusion episodes. In particular, the less intense episode on April 21st and the more intense on June 29th were considered. Figure S2: maps NAAPS and Hysplit back-trajectories for 21st and June 29th, 2022. (*Supplementary Materials*)

References

- [1] K. K. Lee, R. Bing, J. Kiang et al., "Adverse health effects associated with household air pollution: a systematic review, meta-analysis, and burden estimation study," *The Lancet Global Health*, vol. 8, no. 11, pp. e1427–e1434, 2020.
- [2] L. Morawska and W. Huang, "WHO health guidelines for indoor air quality and national recommendations/standards," in *Handbook of Indoor Air Quality*, Y. Zhang, P. K. Hopke, and C. Mandin, Eds., Springer, Singapore, 2022.
- [3] WHO, *Guidelines for Indoor Air Quality, Selected Pollutants*, World Health Organization, Geneva, 2010.
- [4] I. Rivas, J. C. Fussell, F. J. Kelly, and X. Querol, "Indoor Sources of Air Pollutants," in *Indoor Air Pollution*, R. M. Harrison and R. E. Hester, Eds., The Royal Society of Chemistry, 2019.
- [5] A. Cattaneo, A. Spinazzè, and D. M. Cavallo, "Indoor air quality in offices," in *Handbook of Indoor Air Quality*, Y. Zhang, P. K. Hopke, and C. Mandin, Eds., Springer, Singapore, 2022.
- [6] Y. Zou, M. Young, M. Wickey, A. May, and J. D. Clark, "Response of eight low-cost particle sensors and consumer devices to typical indoor emission events in a real home (ASHRAE 1756-RP)," *Science and Technology for the Built Environment*, vol. 26, no. 2, pp. 237–249, 2020.

- [7] S. Magalhaes, J. Baumgartner, and S. Weichenthal, "Impacts of exposure to black carbon, elemental carbon, and ultrafine particles from indoor and outdoor sources on blood pressure in adults: a review of epidemiological evidence," *Environmental Research*, vol. 161, pp. 345–353, 2018.
- [8] M. Scungio, L. Stabile, and G. Buonanno, "Measurements of electronic cigarette-generated particles for the evaluation of lung cancer risk of active and passive users," *Journal of Aerosol Science*, vol. 115, pp. 1–11, 2018.
- [9] S. Patel, S. Sankhyam, E. K. Boedicker et al., "Indoor particulate matter during HOMEChem: concentrations, size distributions, and exposures," *Environmental Science & Technology*, vol. 54, no. 12, pp. 7107–7116, 2020.
- [10] C. W. Lee, T. T. T. Vo, Y. Wee et al., "The adverse impact of incense smoke on human health: from mechanisms to implications," *Journal of Inflammation Research*, vol. 14, pp. 5451–5472, 2021.
- [11] Z. Wang, L. Calderón, A. P. Patton et al., "Comparison of real-time instruments and gravimetric method when measuring particulate matter in a residential building," *Journal of the Air & Waste Management Association*, vol. 66, no. 11, pp. 1109–1120, 2016.
- [12] A. Ruprecht, A. Borgini, C. Veronese et al., "Measurements of particulate matter from electronic and conventional cigarettes: a comparative analysis of methods," *Atmosphere*, vol. 13, no. 9, p. 1393, 2022.
- [13] F. R. Cassee, M. E. Héroux, M. E. Gerlofs-Nijland, and F. J. Kelly, "Particulate matter beyond mass: recent health evidence on the role of fractions, chemical constituents, and sources of emission," *Inhalation Toxicology*, vol. 25, no. 14, pp. 802–812, 2013.
- [14] S. K. Sahu, M. Tiwari, R. C. Bhangare, and G. G. Pandit, "Particle size distribution of mainstream and exhaled cigarette smoke and predictive deposition in human respiratory tract," *Aerosol and Air Quality Research*, vol. 13, no. 1, pp. 324–332, 2013.
- [15] H. Rohra, A. S. Pipal, P. G. Satsangi, and A. Taneja, "Revisiting the atmospheric particles: connecting lines and changing paradigms," *Science of the Total Environment*, vol. 841, article 156676, 2022.
- [16] T. V. Vu, J. Ondracek, V. Zdimal, J. Schwarz, J. M. Delgado-Saborit, and R. M. Harrison, "Physical properties and lung deposition of particles emitted from five major indoor sources," *Air Quality, Atmosphere & Health*, vol. 10, no. 1, pp. 1–14, 2017.
- [17] K. D. Volesky, A. Maki, C. Scherf et al., "The influence of three e-cigarette models on indoor fine and ultrafine particulate matter concentrations under real-world conditions," *Environmental Pollution*, vol. 243, no. Part B, pp. 882–889, 2018.
- [18] A. M. Zarogianni, G. Loupa, and S. Rapsomanikis, "Fragrances and aerosol during office cleaning," *Aerosol and Air Quality Research*, vol. 18, no. 5, pp. 1162–1167, 2018.
- [19] J. Savdie, N. Canha, N. Buitrago, and S. M. Almeida, "Passive exposure to pollutants from a new generation of cigarettes in real life scenarios," *International Journal of Environmental Research and Public Health*, vol. 17, no. 10, p. 3455, 2020.
- [20] J. Tryner, M. Phillips, C. Quinn et al., "Design and testing of a low-cost sensor and sampling platform for indoor air quality," *Building and Environment*, vol. 206, article 108398, 2021.
- [21] J. P. Abbatt and C. Wang, "The atmospheric chemistry of indoor environments," *Environmental Science: Processes & Impacts*, vol. 22, no. 1, pp. 25–48, 2020.
- [22] M. I. Mitova, C. Cluse, D. Correia et al., "Comprehensive air quality assessment of the tobacco heating system 2.2 under simulated indoor environments," *Atmosphere*, vol. 12, no. 8, p. 989, 2021.
- [23] S. Sun, X. Zheng, J. Villalba-Díez, and J. Ordieres-Meré, "Indoor air-quality data-monitoring system: long-term monitoring benefits," *Sensors*, vol. 19, no. 19, p. 4157, 2019.
- [24] I. Demanega, I. Mujan, B. C. Singer, A. S. Andelković, F. Babich, and D. Licina, "Performance assessment of low-cost environmental monitors and single sensors under variable indoor air quality and thermal conditions," *Building and Environment*, vol. 187, article 107415, 2021.
- [25] E. Anastasiou, M. R. Vilcassim, J. Adragna et al., "Feasibility of low-cost particle sensor types in long-term indoor air pollution health studies after repeated calibration, 2019–2021," *Scientific Reports*, vol. 12, no. 1, article 14571, 2022.
- [26] L. Wallace and P. Hopke, "Measuring particle concentration and compositions in indoor air," in *Handbook of Indoor Air Quality*, Y. Zhang, P. K. Hopke, and C. Mandin, Eds., Springer, Singapore, 2021.
- [27] R. E. Connolly, Q. Yu, Z. Wang et al., "Long-term evaluation of a low-cost air sensor network for monitoring indoor and outdoor air quality at the community scale," *Science of the Total Environment*, vol. 807, Part 2, article 150797, 2022.
- [28] Y. Kang, L. Aye, T. D. Ngo, and J. Zhou, "Performance evaluation of low-cost air quality sensors: a review," *Science of the Total Environment*, vol. 818, article 151769, 2022.
- [29] J. Reis, D. Lopes, D. Graça, A. P. Fernandes, A. I. Miranda, and M. Lopes, "Using low-cost sensors to assess real-time comfort and air quality patterns in indoor households," *Environmental Science and Pollution Research*, vol. 30, no. 3, pp. 7736–7751, 2023.
- [30] B. C. Singer and W. W. Delp, "Response of consumer and research grade indoor air quality monitors to residential sources of fine particles," *Indoor Air*, vol. 28, no. 4, pp. 624–639, 2018.
- [31] F. Karagulian, M. Gerboles, M. Barbieri, A. Kotsev, F. Lagler, and A. Borowiak, *Review of sensors for air quality monitoring*, EUR 29826 EN, Publications Office of the European Union, Luxembourg, 2019, JRC116534.
- [32] L. Bai, L. Huang, Z. Wang et al., "Long-term field evaluation of low-cost particulate matter sensors in Nanjing," *Aerosol and Air Quality Research*, vol. 20, no. 2, pp. 242–253, 2020.
- [33] S. Hegde, K. T. Min, J. Moore et al., "Indoor household particulate matter measurements using a network of low-cost sensors," *Aerosol and Air Quality Research*, vol. 20, no. 2, pp. 381–394, 2020.
- [34] M. L. Zamora, J. Rice, and K. Koehler, "One year evaluation of three low-cost PM_{2.5} monitors," *Atmospheric Environment*, vol. 235, article 117615, 2020.
- [35] B. Alfano, L. Barretta, A. Del Giudice et al., "A review of low-cost particulate matter sensors from the developers' perspectives," *Sensors*, vol. 20, no. 23, p. 6819, 2020.
- [36] E. Brattich, A. Bracci, A. Zappi et al., "How to get the best from low-cost particulate matter sensors: guidelines and practical recommendations," *Sensors*, vol. 20, no. 11, p. 3073, 2020.
- [37] M. V. Narayana, D. Jaliha, and S. M. Nagendra, "Establishing a sustainable low-cost air quality monitoring setup: a survey of the state-of-the-art," *Sensors*, vol. 22, no. 1, p. 394, 2022.
- [38] K. K. Barkjohn, B. Gantt, and A. L. Clements, "Development and application of a United States-wide correction for PM

- 2.5 data collected with the PurpleAir sensor,” *Atmospheric Measurement Techniques*, vol. 14, no. 6, pp. 4617–4637, 2021.
- [39] R. Duvall, A. Clements, G. Hagler et al., *Performance testing protocols, metrics, and target values for fine particulate matter air sensors: use in ambient, outdoor, fixed site, non-regulatory supplemental and informational monitoring applications*, U.S. EPA Office of Research and Development, Washington, DC, 2021, EPA/600/R-20/280.
- [40] N. Zimmerman, “Tutorial: guidelines for implementing low-cost sensor networks for aerosol monitoring,” *Journal of Aerosol Science*, vol. 159, article 105872, 2022.
- [41] WMO, *An Update on Low-Cost Sensors for the Measurement of Atmospheric Composition*, World Meteorological Organization, 2021.
- [42] J. Kuula, H. Timonen, J. V. Niemi et al., “Opinion: insights into updating ambient air quality directive 2008/50/EC,” *Atmospheric Chemistry and Physics*, vol. 22, no. 7, pp. 4801–4808, 2022.
- [43] S. Yarkin, M. Gerboles, A. Borowiak et al., “Modified target diagram to check compliance of low-cost sensors with the data quality objectives of the European air quality directive,” *Atmospheric Environment*, vol. 273, article 118967, 2022.
- [44] H. Chojer, P. T. B. S. Branco, F. G. Martins, M. C. M. Alvim-Ferraz, and S. I. V. Sousa, “Development of low-cost indoor air quality monitoring devices: recent advancements,” *Science of the Total Environment*, vol. 727, article 138385, 2020.
- [45] M. R. Giordano, C. Malings, S. N. Pandis et al., “From low-cost sensors to high-quality data: a summary of challenges and best practices for effectively calibrating low-cost particulate matter mass sensors,” *Journal of Aerosol Science*, vol. 158, article 105833, 2021.
- [46] J. P. Sá, M. C. M. Alvim-Ferraz, F. G. Martins, and S. I. Sousa, “Application of the low-cost sensing technology for indoor air quality monitoring: a review,” *Environmental Technology & Innovation*, vol. 28, article 102551, 2022.
- [47] M. Ródenas García, A. Spinazzé, P. T. Branco et al., “Review of low-cost sensors for indoor air quality: features and applications,” *Applied Spectroscopy Reviews*, vol. 57, no. 9-10, pp. 747–779, 2022.
- [48] F. M. J. Bulot, H. S. Russell, M. Rezaei et al., “Laboratory comparison of low-cost particulate matter sensors to measure transient events of pollution,” *Sensors*, vol. 20, no. 8, p. 2219, 2020.
- [49] J. Kuula, T. Mäkelä, M. Aurela et al., “Laboratory evaluation of particle-size selectivity of optical low-cost particulate matter sensors,” *Atmospheric Measurement Techniques*, vol. 13, no. 5, pp. 2413–2423, 2020.
- [50] R. Caggiano, M. Macchiato, and S. Trippetta, “Levels, chemical composition, and sources of fine aerosol particles (PM₁) in an area of the Mediterranean basin,” *Science of the Total Environment*, vol. 408, no. 4, pp. 884–895, 2010.
- [51] M. Calvello, F. Esposito, G. Pavese, and C. Serio, “Physical and optical properties of atmospheric aerosols by in-situ and radiometric measurements,” *Atmospheric Chemistry and Physics*, vol. 10, no. 5, pp. 2195–2208, 2010.
- [52] A. Boselli, R. Caggiano, C. Cornacchia et al., “Multi year sun-photometer measurements for aerosol characterization in a Central Mediterranean site,” *Atmospheric Research*, vol. 104-105, pp. 98–110, 2012.
- [53] G. Pavese, M. Calvello, and F. Esposito, “Black carbon and organic components in the atmosphere of Southern Italy: comparing emissions from different sources and production processes of carbonaceous particles,” *Aerosol and Air Quality Research*, vol. 12, no. 6, pp. 1146–1156, 2012.
- [54] G. Pavese, F. Agresti, M. Calvello, F. Esposito, and A. Lettino, “Outdoor and indoor measurements of number particles size distributions and equivalent black carbon (EBC) at a mechanical manufacturing plant,” *Atmospheric Pollution Research*, vol. 13, no. 8, article 101488, 2022.
- [55] S. V. Hering, G. S. Lewis, S. R. Spielman et al., “Detection near 1-nm with a laminar-flow, water-based condensation particle counter,” *Aerosol Science and Technology*, vol. 51, no. 3, pp. 354–362, 2017.
- [56] “Sensirion SPS30 Sensor Specification,” December 2022, <https://www.sensirion.com/en/download-center/particulate-matter-sensors-pm/particulate-matter-sensor-sps30/>.
- [57] J. Tryner, J. Mehaffy, D. Miller-Lionberg, and J. Volckens, “Effects of aerosol type and simulated aging on performance of low-cost PM sensors,” *Journal of Aerosol Science*, vol. 150, article 105654, 2020.
- [58] M. Calvello, F. Esposito, M. Lorusso, and G. Pavese, “A two-year database of BC measurements at the biggest European crude oil pre-treatment plant: a comparison with organic gaseous compounds and PM₁₀ loading,” *Atmospheric Research*, vol. 164-165, pp. 156–166, 2015.
- [59] May 2023, <https://www.stradeanas.it/sites/default/files/Anas%20Dati%20TGMA%202017.pdf>.
- [60] L. Stabile, F. C. Fuoco, and G. Buonanno, “Characteristics of particles and black carbon emitted by combustion of incenses, candles, and anti-mosquito products,” *Building and Environment*, vol. 56, pp. 184–191, 2012.
- [61] B. Višić, E. Kranjc, L. Pirker et al., “Incense powder and particle emission characteristics during and after burning incense in an unventilated room setting,” *Air Quality, Atmosphere & Health*, vol. 11, no. 6, pp. 649–663, 2018.
- [62] R. K. Chakrabarty, I. J. Arnold, D. M. Francisco et al., “Black and brown carbon fractal aggregates from combustion of two fuels widely used in Asian rituals,” *Journal of Quantitative Spectroscopy and Radiative Transfer*, vol. 122, pp. 25–30, 2013.
- [63] M. Gyawali, W. P. Arnott, R. A. Zaveri et al., “Photoacoustic optical properties at UV, VIS, and near IR wavelengths for laboratory generated and winter time ambient urban aerosols,” *Atmospheric Chemistry and Physics*, vol. 12, no. 5, pp. 2587–2601, 2012.
- [64] H. A. Mulder, J. L. Patterson, M. S. Halquist et al., “The effect of electronic cigarette user modifications and e-liquid adulteration on the particle size profile of an aerosolized product,” *Scientific Reports*, vol. 9, no. 1, article 10221, 2019.
- [65] H. A. Mulder, J. B. Stewart, I. P. Blue et al., “Characterization of E-cigarette coil temperature and toxic metal analysis by infrared temperature sensing and scanning electron microscopy–energy-dispersive X-ray,” *Inhalation Toxicology*, vol. 32, no. 13-14, pp. 447–455, 2020.
- [66] A. Pacitto, L. Stabile, M. Scungio, V. Rizza, and G. Buonanno, “Characterization of airborne particles emitted by an electrically heated tobacco smoking system,” *Environmental Pollution*, vol. 240, pp. 248–254, 2018.
- [67] M. Peruzzi, E. Cavarretta, G. Frati et al., “Comparative indoor pollution from Glo, Iqos, and Juul, using traditional combustion cigarettes as benchmark: evidence from the randomized SUR-VAPES AIR trial,” *International Journal of Environmental Research and Public Health*, vol. 17, no. 17, p. 6029, 2020.

- [68] C. Protano, M. Manigrasso, V. Cammalleri et al., “Impact of electronic alternatives to tobacco cigarettes on indoor air particulate matter levels,” *International Journal of Environmental Research and Public Health*, vol. 17, no. 8, p. 2947, 2020.
- [69] D. Gallart-Mateu, Z. Dhaouadi, and M. de la Guardia, “Exposure of heat-not-burn tobacco effect on the quality of air and expiratory plume,” *Microchemical Journal*, vol. 170, article 106733, 2021.
- [70] M. Meišutovič-Akhtarjeva, T. Prasauskas, D. Čiužas, V. Kaunelienė, and D. Martuzevičius, “The dynamics of exhaled aerosol following the usage of heated tobacco product, electronic cigarette, and conventional cigarette,” *Aerosol and Air Quality Research*, vol. 21, no. 8, article 200653, 2021.
- [71] T. Kärkelä, U. Tapper, and T. Kajolinna, “Comparison of 3R4F cigarette smoke and IQOS heated tobacco product aerosol emissions,” *Environmental Science and Pollution Research*, vol. 29, pp. 27051–27069, 2021.
- [72] E. L. Floyd, L. Queimado, J. Wang, J. L. Regens, and D. L. Johnson, “Electronic cigarette power affects count concentration and particle size distribution of vaping aerosol,” *PLoS One*, vol. 13, no. 12, article e0210147, 2018.
- [73] M. Manigrasso, C. Protano, M. Vitali, and P. Avino, “Passive vaping from sub-ohm electronic cigarette devices,” *International Journal of Environmental Research and Public Health*, vol. 18, no. 21, article 11606, 2021.
- [74] M. Williams, A. Villarreal, K. Bozhilov, S. Lin, and P. Talbot, “Metal and silicate particles including nanoparticles are present in electronic cigarette cartomizer fluid and aerosol,” *PLoS One*, vol. 8, no. 3, article e57987, 2013.
- [75] M. Williams, K. Bozhilov, S. Ghai, and P. Talbot, “Elements including metals in the atomizer and aerosol of disposable electronic cigarettes and electronic hookahs,” *PLoS One*, vol. 12, no. 4, article e0175430, 2017.
- [76] P. Olmedo, W. Goessler, S. Tanda et al., “Metal concentrations in e-cigarette liquid and aerosol samples: the contribution of metallic coils,” *Environmental Health Perspectives*, vol. 126, no. 2, article 027010, 2018.
- [77] S. Sousan, K. Koehler, L. Hallett, and T. M. Peters, “Evaluation of consumer monitors to measure particulate matter,” *Journal of Aerosol Science*, vol. 107, pp. 123–133, 2017.
- [78] M. Badura, P. Batog, A. Drzeniecka-Osiadacz, and P. Modzel, “Evaluation of low-cost sensors for ambient PM_{2.5} monitoring,” *Journal of Sensors*, vol. 2018, Article ID 5096540, 16 pages, 2018.
- [79] F. M. Bulot, S. J. Johnston, P. J. Basford et al., “Long-term field comparison of multiple low-cost particulate matter sensors in an outdoor urban environment,” *Scientific Reports*, vol. 9, no. 1, pp. 1–13, 2019.
- [80] S. Sousan, S. Regmi, and Y. M. Park, “Laboratory evaluation of low-cost optical particle counters for environmental and occupational exposures,” *Sensors*, vol. 21, no. 12, p. 4146, 2021.
- [81] “South Coast Air Quality Management District (SCAQMD): Field evaluation Sensirion SPS30 evaluation kit background,” November 2022, <http://www.aqmd.gov/docs/default-source/aq-spec/field-evaluations/sensirion-sps30-evaluation-kit-field-evaluation.pdf>.